Reconfigurable continuous-zoom metalens in visible band

Yuan Cui (崔 圆)¹, Guoxing Zheng (郑国兴)¹,², Ming Chen (陈 明)³, Yilun Zhang (张逸伦)³,
Yan Yang (杨 妍)⁴, Jin Tao (陶 金)², Taotao He (何桃桃)¹, and Zile Li (李子乐)¹,²,*

¹*Electronic Information School, Wuhan University, Wuhan 430072, China*

²*NOEIC, State Key Laboratory of Optical Communication Technologies and Networks,*
Wuhan Research Institute of Posts and Telecommunications, Wuhan 430074, China

³*Photonics Research Centre, Guilin University of Electronic Technology, Guilin 541004, China*

⁴*Integrated Circuit Advanced Process Center, Institute of Microelectronics of Chinese Academy of Sciences,*
Beijing 100029, China

*Corresponding author: lizile@whu.edu.cn

The design of a conventional zoom lens is always challenging because it requires not only sophisticated optical design strategy, but also complex and precise mechanical structures for system adjustment. Here, we propose a continuous-zoom lens consisting of two chiral geometric metasurfaces with dielectric nanobrick arrays sitting on a transparent substrate. The metalens can continuously vary the focal length by rotating either of the two metasurfaces around its optical axis without changing any other conditions. Due to the polarization dependence of the geometric metasurface, the positive and negative polarities are interchangeable in one identical metalens only by changing the handedness of the incident circularly polarized light, which can generate varying focal lengths ranging from −∞ to +∞ in principle.

OCIS codes: 160.3918, 160.4670.
doi: 10.3788/COL201917.111603.

By virtue of the capability of manipulating the electromagnetic fields, metasurfaces[1–8] are widely used to develop many new optical devices and optimize traditional optical devices. In particular, geometric metasurfaces (GEMSs) get extensive attraction due to their precise phase control ability. The beauty of this approach lies in the linear dependence of phase delay φ on the orientation angle ϕ of each nanostructure, i.e., $\varphi = \pm 2\phi$[9–11]; the sign is determined by the polarization state of incident circularly polarized (CP) light. More importantly, the scattering amplitude remains unchanged since the geometric nanostructure remains consistent. Therefore, GEMSs offer new perspectives in designing complex phase-only optical elements, such as holograms[12–20] and metalenses[21,22]. As one of the most important optical functionalities, continuous zoom has been widely valued by researchers, which is currently combined with metasurfaces to present a lot of designs. A stretching metalens on a flexible substrate with a limited zoom range of 1.5 cm has been reported recently, but its zoom range is hard to get broader[23]. An Alvarez metalens realizes a broader zoom range by lateral actuation, which means that a large zoom range always accompanies the expense of space[24]. The tunable metalens using microelectromechanical systems (MEMS) zooms by actuating a compound system axially while it can only cover a zoom range of 64 μm[25]. These zoom metalenses mentioned above have not done much work in terms of zoom range, and it is still not an easy task to tune focal length over a wide range for a metalens.

Recently, researchers have proposed the Moiré effect[26,27] combined with diffractive optical elements (DOEs)

to realize zooming by relatively rotating two DOEs[28,29]. In this Letter, we further verify that the Moiré effect can be realized by the combination of two chiral GEMSs, and they can be used to form a continuous-zoom metalens. More interestingly, due to the polarization dependence[30–35] of a GEMS, the zoom range of the compound metalens can further be extended to −∞–+∞, which indicates that we can shape a beam of incident light into a convergent, divergent, or plane wave with any spherical radius in principle. Considering its advantages of ultra-compactness, continuous zooming, and easiness for adjustment and fabrication, the proposed continuous-zoom metalens can provide new perspectives and a practical method for wide-range and reconfigurable beam wavefront steering in an ultra-simple way.

The working principle of a continuous-zoom metalens consisting of two GEMSs is shown in Fig. 1(a). By rotating two GEMSs relatively, the focal length of the compound metalens varies continuously, and the incident CP light can be focused on the image plane of the metalens. To form the two GEMSs, we use transmissive metasurfaces constructed by dielectric silicon nanobrick arrays sitting on a silicon dioxide substrate. The nanobrick arrays have the same dimension with length L, width W, height H, and unit-cell size C, as shown in Fig. 1(b). Each nanobrick acts as a half-wave plate[15,36,37], and it can transform the incident CP light into the opposite polarization state accompanied by a geometric phase delay φ ($\varphi = \pm 2\phi$). Since the nanobrick's orientation angle can be designed in $[0, \pi]$, the geometric phase is continuously and accurately controlled in $[0, 2\pi]$ by assigning different orientation angles,
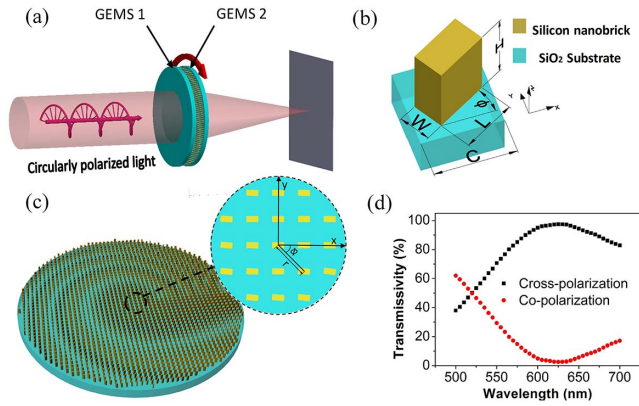
Fig. 1. (a) Working principle of a continuous-zoom metalens. (b) Diagram of a nanobrick unit structure. Each nanobrick was designed with length $L = 140$ nm, width $W = 70$ nm, height $H = 350$ nm, and cell size $C = 300$ nm at an operation wavelength of 633 nm. ϕ is the orientation angle of the nanobrick, and the incident light propagates along the z-axis direction. (c) Schematic diagram of one of the designed GEMSs. (d) The co-polarization and cross-polarization transmissivities of a nanobrick. The simulation was run by normally illuminating a nanobrick with a beam of CP light and under the boundary condition of a period.

which will bring great freedoms for designing phase-only devices such as lenses. The geometry of a nanobrick was designed and simulated by commercial electromagnetic simulation software (COMSOL). To simulate the effect of a single nanobrick in an array, a periodic boundary condition was used in the modeling process. The nanobrick was illuminated by CP light, and we swept the nanobrick's dimension and cell size at an operation wavelength of 633 nm to optimize the performance. As shown in Fig. 1(d), the transmitted light consists of two circular polarization states: cross-polarization with a phase delay φ has the opposite handedness to that of the incident CP light, while the co-polarization has the same handedness without phase delay. This configuration with optimized dimension maintains a fairly large transmissivity of cross-polarization over 95%, and the undesired co-polarization is extremely low, which means that each nanobrick as a sub-wavelength half-wave plate leads to a nearly complete conversion between two opposite circular polarization states, and the co-polarized light as background light will not have a large impact on the performance of the device.

For a Moiré diffractive lens, the transmission functions of two phase plates can be described as[28,38,39]

$$T_1(r, \Phi) = \exp(iar^2\Phi) \tag{1}$$

and

$$T_2(r, \Phi) = \exp(-iar^2\Phi), \tag{2}$$

where r is the radius from an arbitrary point to the center of the phase plate, Φ is the angle between the x axis and the line where the point is located to the center, as shown

in Fig. 1(c), and a is a constant. If we use GEMSs to form the two phase plates, due to the polarization dependence of a GEMS, the left-handed CP (LCP) incident light will be converted into right-handed CP (RCP) light after passing through the first GEMS, that is, the second GEMS is illuminated by a beam of RCP light. Since the two equations are complex conjugates, and the signs of the phase change amount generated by LCP and RCP states are reversed, it is interesting that the two GEMSs can be designed with the same orientation angle distribution of nanobricks. If we combine two GEMSs face to face, as shown in Fig. 1(a), the two nanobrick arrays should be chiral.

When the second GEMS is rotated by a mutual angle ϑ around its optical axis, the transmission function T_2 is converted to

$$T_{2,rot}(r, \Phi) = \exp[-iar^2(\Phi - \theta)]. \tag{3}$$

Therefore, the transmission function of the metalens is

$$T_{com} = T_1(r, \Phi)\, T_{2,rot}(r, \Phi) = \exp(ia\theta r^2). \tag{4}$$

Compared with the transmission function of a spherical lens, namely,

$$T_{lens} = \exp\left(i\frac{\pi r^2}{\lambda f}\right), \tag{5}$$

where λ is the operation wavelength, and f is the focal length of a lens. The focal length of the metalens satisfies

$$f = \frac{\pi}{a\theta\lambda} \text{ for LCP incident light,} \tag{6}$$

and

$$f = -\frac{\pi}{a\theta\lambda} \text{ for RCP incident light.} \tag{7}$$

From Eqs. (6) and (7), we can observe that when the constant a and the incident wavelength λ are determined, the focal length will only depend on the mutual rotation angle θ, in other words, the zoom functionality of the continuous-zoom metalens can be achieved by mutually rotating two GEMSs. The focal length verus rotation angle is shown in Fig. 2. Due to the polarization dependence of a GEMS, if the metalens is designed as a positive lens at LCP light incidence, it will become a negative lens when we change the polarization state of the incident light and vice versa. The most important thing is that it can make the focal length of the metalens switch instantaneously from a positive value to a negative one whilst retaining the same absolute value by changing the handedness of the CP incident light. It is known that a beam of incident light with any polarized state can be a linear combination of LCP and RCP, and thus the positive and negative focal spots will appear simultaneously when non-CP light is incident. However, because of the periodicity of the mutual
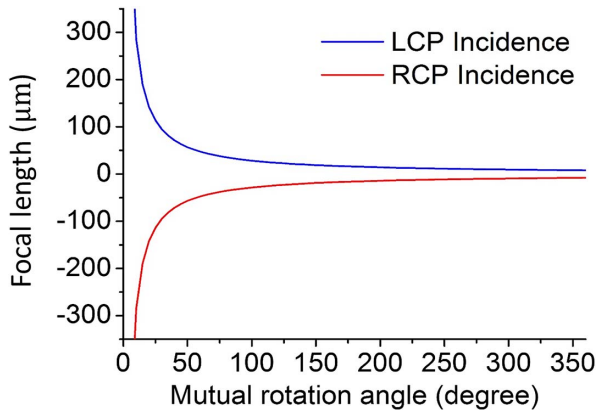
Fig. 2. Focal length of the metalens as a function of the mutual rotation angle between two GEMSs. With LCP incident light, the metalens acts as a positive zoom lens and its focal length changes from $+\infty$ to nearly zero like the blue curve. When the incident light is switched to RCP, the metalens becomes a negative one, and its focal length ranges from $-\infty$ to nearly zero. In this example, the metalens dimension is 30.3 μm × 30.3 μm, the constant a is 0.1 μm^{-2}, and the operation wavelength is 633 nm.

rotation, there is a discontinuous spot at 0° or say 360°, and the result at this angle can only be described as no focusing or focusing on infinity.

In Eqs. (6) and (7), the constant a, which is limited by the resolution of a GEMS, depends on the pixel size and the maximum radius of the GEMS, and its constraint can be expressed by[28]

$$a < \frac{1}{2Cr_{max}}, \qquad (8)$$

where C is the cell size of a nanobrick structure, and r_{max} is the radius of the GEMS.

According to Eqs. (6) and (7), we can find that the minimum value of the focal length f is related to the cell size C and the GEMSs' radius r_{max}. For example, with a pixel size of 300 nm × 300 nm, lens dimension of 3.3 μm × 3.3 μm (11 × 11 pixels), and operation wavelength of 633 nm, the minimum focal length is calculated to be a value of only 780 nm when θ is near 360°. This value (780 nm) is even close to the wavelength, and we can consider that it is almost zero in this working condition. However, because of the periodicity shown in Eq. (4), in addition to the desired sector, there is another sector that takes up a part of incident light power, and the scale of this undesired sector is proportional to θ[28]. As a consequence, the energy concentrated in the focal spot decreases as the mutual rotation angle θ keeps increasing. In order to ensure that the metalens satisfies the request of enough focal spot energy, we set the maximum angle of θ to 180°, and the value of minimum focal length becomes 1.56 μm, which is still an extremely short length, close to twice that of the operation wavelength. On the other hand, if the metalens is designed by Eq. (6) with a positive

focal length, we can easily observe that the focal length can be extended to $+\infty$ when θ is near 0°. Therefore, by rotating one GEMS, the metalens can cover a focal length ranging from $+\infty$ to an extremely short length. More importantly, only by changing the handedness of CP incident light, the focal length can cover nearly $-\infty$–0. Finally, we can obtain a continuous-zoom metalens, which contains a varying focal length almost from $-\infty$ to $+\infty$ (except for a relatively short gap) only by rotating any one of the GEMSs around its optical axis.

For practice, we designed a continuous-zoom metalens and simulated the light propagation with a beam of normally incident CP light by using the commercial electromagnetic simulation software package (FDTD Solutions). The three-dimensional (3D) finite-difference time-domain method was used in the simulations, and the boundary condition was perfect matching layers (PML). The two GEMSs of the simulated metalens with phase distribution of $\Phi = a\theta r^2$ have a cell size of 300 nm × 300 nm, aperture dimension of 30.3 μm × 30.3 μm, and a constant a of 0.1 μm^{-2}, operating at a wavelength of 633 nm. The simulation results are shown in Fig. 3. Due to the limitations of computation resource and time, we can only simulate a small aperture metalens at several selected rotation angles.

The fact is that it is a mostly ideal state when two phase profiles of GEMSs overlay completely and are centered perfectly. However, for the purpose of continuous zooming by rotating, the two GEMSs are separated by a distance of
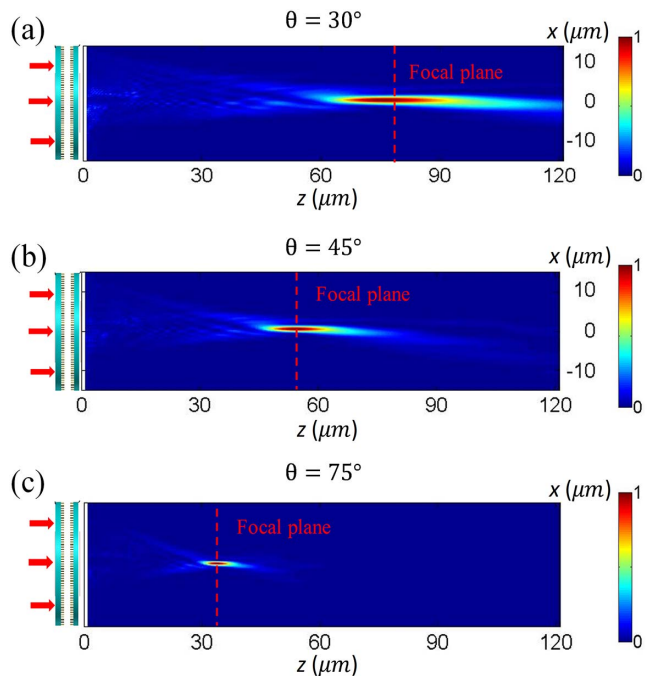

Fig. 3. Simulation of a zoom metalens. Full-wave numerical simulations were performed by FDTD Solutions for the propagation of LCP incident light. (a)–(c) Intensity of the electric field along the direction of light propagation (z axis) corresponding to $\theta = 30°$, 45°, and 75°, respectively. The back surface of the metalens is placed at $z = 0$ μm.

140 nm, which brings about the transmitted light deviating slightly from the optical axis, and such out of symmetry also stems from the phase distribution of each GEMS not being centrally symmetric. The intensity distribution of the electric field in three situations (θ is 30°, 45°, and 75°, respectively) indicates excellent light focusing without noise spots, shown in Figs. 3(a)–3(c). It is observed that the focal planes of $\theta = 30°$, 45°, and 75° have different deviations from 94.8 μm, 63.2 μm, and 37.9 μm calculated theoretically by Eq. (6). Because of the coupling effect among adjacent nanobricks and the finite aperture of the metalens[40,41], such deviation will decrease as the mutual rotation angle θ increases or say the focal length decreases. Although the simulated focal plane is not at an ideal place, it does not affect the zoom functionality of a large range, since the mutual rotation angle θ is reconfigurable, and all the simulation results show that the metalens can focus light well. In a practical application, we can calibrate the exact focal length for different mutual rotation angles. In addition, the alignment error may exist if two GEMSs of the metalens are decentered, and such misalignment would decrease the efficiency and deteriorate the effect of imaging.

The calculated focusing efficiencies (i.e., the ratio of focal spot energy at the focal plane and incident energy) of the metalens are 35.92%, 32.92%, and 26.67%, corresponding to $\theta = 30°$, 45°, and 75°, respectively, which agree well with the correlative relationship between focal spot energy and the mutual rotation angle of the metalens. When the operation wavelength deviates from 633 nm, the metalens will suffer from inefficiency of focusing because the energy of cross-polarized light decreases [see Fig. 1(d)].

The resolution of a metalens is determined by the diffraction limit with

$$\sigma = \frac{0.61\lambda}{NA}, \tag{9}$$

where NA is the numerical aperture of the metalens. On the basis of Eq. (9), a metalens with a longer focal length corresponds to a smaller NA and would produce a larger spot for the same lens aperture. In Figs. 4(a)–4(c), for the same aperture (30.3 μm), the focal spot size at the focal plane of the optical system varies with different focal
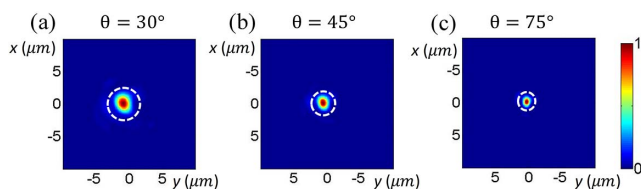

Fig. 4. Simulation results at the focal plane of the metalens. (a)–(c) Intensity of the electric field at the cross-section of the focal plane corresponding to $\theta = 30°$, 45°, and 75°, respectively. The Airy disks marked by white curves are calculated with the diffraction limit principle, and their radii are 2.42 μm ($\theta = 30°$), 1.61 μm ($\theta = 45°$), and 0.97 μm ($\theta = 75°$), respectively.
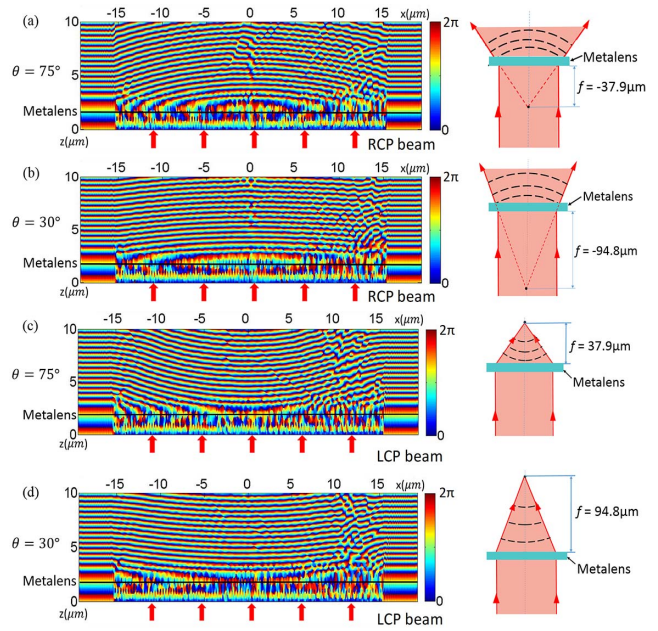

Fig. 5. Simulation of a zoom metalens. (a), (b) The simulation domains show the distribution of phase along the direction of light propagation (z axis) for $\theta = 75°$ ($f = -37.9$ μm) and $\theta = 30°$ ($f = -94.8$ μm), respectively. (c), (d) Compared with the negative focal length case, the simulation domains show the phase distribution of $\theta = 75°$ ($f = 37.9$ μm) and $\theta = 30°$ ($f = 94.8$ μm) with LCP light incidence.

lengths, which keeps consistent with the diffraction limit principle.

The simulation results in Fig. 5 show that the metalens transforms from a positive lens to a negative one when the polarization state of incident light is changed from LCP to RCP, i.e., the focal length of $\theta = 75°$ changes from 37.9 μm to -37.9 μm in Fig. 5(a), and the focal length 94.8 μm of $\theta = 30°$ becomes -94.8 μm in Fig. 5(b). The simulation results reveal that incident light passing through the metalens does not focus anymore, and the curvature radii of wave fronts corresponding to 75° and 30° are approximately 41.2 μm and 109.6 μm, respectively. It turns out that the output light behind the metalens is divergent in image space, and its negative focal length also can be adjusted continuously by changing the mutual rotation angle. In contrast to the negative focusing, Figs. 5(c) and 5(d) show the situations of positive focusing when θ is 75° and 30°. This confirms that the focal length of the metalens described in this Letter can cover a fairly large dynamic range by rotating two chiral GEMSs of a metalens and changing the polarization state of incident light.

It is known that the metalens obtains the maximum focusing energy at $\theta = 0°$; however, the focal length is infinity, which does not satisfy practical requirements. The contradiction between the focusing energy and the focal range can be solved by adding a constant phase compensation[38], and the transmission functions become

$$T_1(r, \Phi) = \exp(iar^2\Phi + ibr^2) \tag{10}$$

and

$$T_2(r, \Phi) = \exp(-iar^2\Phi + ibr^2), \qquad (11)$$

where b is a constant. Therefore, a new combination metalens with a mutual rotation θ can be described as

$$T_{com}(r, \Phi) = \exp(-iar^2\theta + i2br^2). \qquad (12)$$

The focal length of the corrected metalens becomes

$$f = \frac{\pi}{(a\theta + 2b)\lambda} \text{ for LCP incident light,} \qquad (13)$$

and

$$f = -\frac{\pi}{(a\theta + 2b)\lambda} \text{ for RCP incident light.} \qquad (14)$$

In Eqs. (13) and (14), it demonstrates that the focal length reaches its maximum at $\theta_{min} = -2b/a$, and the constant b depends on the selection of θ_{min}. On the other hand, the maximum diffraction efficiency is still generated at $\theta = 0°$.

To further verify zoom functionality of the corrected metalens, we assume that the mutual rotation angle θ increases from $-90°$, that is, the focal length reaches a maximum at $-90°$, which means that the constant b in Eqs. (13) and (14) equals $a\pi/4$. To show the overall range variation of the focal length versus θ, we selected four certain mutual rotation angles θ, which are $-90°$, $-45°$, $0°$, and $45°$, respectively. The four simulation results in Fig. 6 show that the focal length of the corrected metalens changes from $-\infty$ to a relatively short one. By means of introducing phase compensation, the incident light is focused at infinity when $\theta = 90°$, which is different from the original metalens that focuses light to infinity at $\theta = 0°$. Instead, the focal length is reduced to 31.5 µm at $\theta = 0°$. For the focal spots at three different focal planes of $\theta = -45°$, $0°$, and $45°$, the calculated focusing efficiencies are 27.37%, 37.68%, and 26.61%, respectively.

Furthermore, the corrected metalens still has the functionality of polarization control, namely, as a beam of incident light converts its polarization state into an opposite one, the polarity of the metalens also switches rapidly between a positive one and a negative one. We assume that the positive and negative focusing efficiencies are both less than our requirement when θ is greater than 180°; then, the zoom range of the corrected metalens is broader than that of the original one within the required efficiency.

The proposed continuous-zoom metalens designed with two GEMSs has great advantages over the previously proposed zoom diffractive lenses. Firstly, the pixel size of GEMS is at a sub-wavelength level so that the phase profile of a metalens is much finer. In this Letter, each pixel size is 300 nm × 300 nm, which is smaller than half of a wavelength and can provide a relatively high resolution and information density. Secondly, the metalens based on GEMSs can manipulate phase continuously, which makes the phase distribution more continuous and the process of zooming smoother. Thirdly, compared with most of the existing continuous-zoom metalenses, the metalens we proposed does not require any spatial extension like lateral or axial displacement, which provides a better implementation for ultra-thin and reliable imaging systems. Finally, because of the polarization dependence of a GEMS, the positive and negative polarities are interchangeable in one identical metalens only by changing the handedness of the incident CP light. Therefore, we can manipulate the focal length of a metalens in a large dynamic range but not at the expense of increasing complexity of an imaging system. Additionally, such a wide zoom range has never been implemented by previously proposed metalenses.

The high integration and simple structure of the reconfigurable continuous-zoom metalens make it promising in consumer electronics. It can be used as an integrated camera in mobile phones and smart devices. It can also be integrated into 3D light sensing equipment to flexibly adjust the imaging range, making it easier to be used in 3D sensing applications. The above zoom technology can be
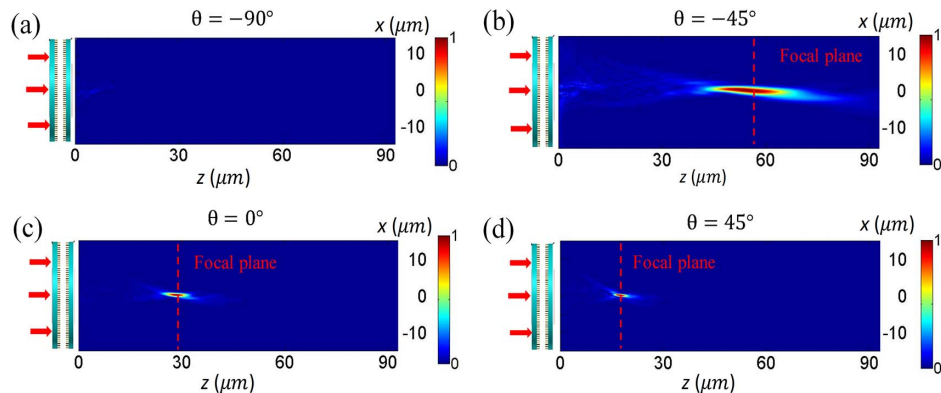

Fig. 6. A variation tendency of the focal length for the corrected metalens. (a)–(d) Intensity of the electric field along the direction of light propagation (z axis) corresponding to $\theta = -90°$ ($f = +\infty$), $\theta = -45°$ ($f = 63.1$ µm), $\theta = 0°$ ($f = 31.5$ µm), and $\theta = 45°$ ($f = 21.0$ µm), respectively. The corrected metalens is illuminated by a beam of LCP incident light.

further extended, such as a microwave scanning antenna, which can realize continuous and flexible switching of the microwave in different fields of view.

In summary, we propose a continuous-zoom metalens, which is composed of only two metasurface-based phase plates with precise phase modulation and ultra-compact structures. The zooming process is realized by mutually rotating two GEMSs, which is simple in operation and fast in response. Besides, the metalens can provide fairly high information density and finer phase distribution, and the focal length can almost vary from $-\infty$ to $+\infty$ without spatial extension in any direction or additional equipment. Compared with conventional DOE-based zoom lens, the metasurfaces are two-dimensional (2D) planar material, so they do not require the multi-step design and process. With such a miniaturized structure and simple design, the zoom metalens can be applied to many optical imaging systems with ultra-compact and continuous-zoom requirements.

References

1. N. Yu, P. Genevet, M. A. Kats, F. Aieta, J. P. Tetienne, F. Capasso, and Z. Gaburro, Science **334**, 333 (2011).
2. S. Sun, Q. He, S. Xiao, Q. Xu, X. Li, and L. Zhou, Nat. Mater. **11**, 426 (2012).
3. C. Sheng, H. Liu, H. Chen, and S. Zhu, Nat. Commun. **9**, 4271 (2018).
4. G. Zheng, G. Liu, M. G. Kenney, Z. Li, P. A. He, S. Li, Z. Ren, and Q. Deng, Opt. Express **24**, 6749 (2016).
5. H. Sun, Y. Zhang, K. Wang, Y. Zhao, W. Kou, S. Liang, J. Han, and Z. Yang, Chin. Opt. Lett. **16**, 081601 (2018).
6. Q. Yang, X. Chen, Q. Xu, C. Tian, Y. Xu, L. Cong, X. Zhang, Y. Li, C. Zhang, and X. Zhang, Photon. Res. **6**, 1056 (2018).
7. Z. Yin, F. Chen, L. Zhu, K. Guo, F. Shen, Q. Zhou, and Z. Guo, J. Mater. Chem. C **6**, 6354 (2018).
8. J. Yan, Y. Guo, M. Pu, X. Li, X. Ma, and X. Luo, Chin. Opt. Lett. **16**, 050003 (2018).
9. Z. Li, Q. Dai, M. Q. Mehmood, G. Hu, B. L. Yanchuk, J. Tao, C. Hao, I. Kim, H. Jeong, G. Zheng, S. Yu, A. Alù, J. Rho, and C.-W. Qiu, Light Sci. Appl. **7**, 63 (2018).
10. F. Yue, X. Zang, D. Wen, Z. Li, C. Zhang, H. Liu, B. D. Gerardot, W. Wang, G. Zheng, and X. Chen, Sci. Rep. **7**, 11440 (2017).
11. M. Khorasaninejad and K. B. Crozier, Nat. Commun. **5**, 5386 (2014).
12. L. Li, T. J. Cui, W. Ji, S. Liu, J. Ding, X. Wan, Y. B. Li, M. Jiang, C.-W. Qiu, and S. Zhang, Nat. Commun. **8**, 197 (2017).
13. G. Zheng, H. M̈hlenbernd, M. Kenney, G. Li, T. Zentgraf, and S. Zhang, Nat. Nanotechnol. **10**, 308 (2015).
14. Z. Deng, J. Deng, X. Zhuang, S. Wang, T. Shi, G. P. Wang, Y. Wang, J. Xu, Y. Cao, and X. Wang, Light Sci. Appl. **7**, 78 (2018).
15. J. Li, S. Kamin, G. Zheng, F. Neubrech, S. Zhang, and N. Liu, Sci. Adv. **4**, r6768 (2018).
16. J. Deng, Z. Li, G. Zheng, J. Tao, Q. Dai, L. Deng, P. He, Q. Deng, and Q. Mao, Opt. Express **26**, 11843 (2018).
17. Z. Li, I. Kim, L. Zhang, M. Q. Mehmood, M. S. Anwar, M. Saleem, D. Lee, K. T. Nam, S. Zhang, B. Luk'yanchuk, Y. Wang, G. Zheng, J. Rho, and C.-W. Qiu, ACS Nano **11**, 9382 (2017).
18. D. Wen, F. Yue, G. Li, G. Zheng, K. Chan, S. Chen, M. Chen, K. F. Li, P. W. Wong, and K. W. Cheah, Nat. Commun. **6**, 8241 (2015).
19. H. C. Liu, B. Yang, Q. Guo, J. Shi, C. Guan, G. Zheng, H. M̈hlenbernd, G. Li, T. Zentgraf, and S. Zhang, Sci. Adv. **3**, e1701477 (2017).
20. I. Kim, G. Yoon, J. Jang, P. Genevet, K. T. Nam, and J. Rho, ACS Photonics **5**, 3876 (2018).
21. H. Zhu, T. Xu, Z. Wang, J. Li, Z. Hang, L. Zhou, S. Chen, X. Li, and L. Chen, Opt. Express **26**, 28531 (2018).
22. D. Wen, F. Yue, W. Liu, S. Chen, and X. Chen, Adv. Opt. Mater. **6**, 1800348 (2018).
23. A. She, S. Zhang, S. Shian, D. R. Clarke, and F. Capasso, Sci. Adv. **4**, p9957 (2018).
24. A. Zhan, A. Majumdar, and S. Colburn, Optica **5**, 825 (2018).
25. E. Arbabi, A. Arbabi, S. M. Kamali, Y. Horie, M. Faraji-Dana, and A. Faraon, Nat. Commun. **9**, 812 (2018).
26. Z. Wu and Y. Zheng, Adv. Opt. Mater. **6**, 1701057 (2018).
27. J. Han, I. Kim, J. Ryu, J. Kim, J. Cho, G. Yim, H. Park, B. Min, and M. Choi, Opt. Express **23**, 17443 (2015).
28. S. Bernet and M. Ritsch-Marte, Appl. Opt. **47**, 3722 (2008).
29. Z. Jaroszewicz, A. Kolodziejczyk, A. Mira, R. Henao, and S. Bará, Opt. Express **13**, 918 (2005).
30. Z. Li, G. Zheng, P. He, S. Li, Q. Deng, J. Zhao, and Y. Ai, Opt. Lett. **40**, 4285 (2015).
31. F. Zhong, J. Li, H. Liu, and S. Zhu, Phys. Rev. Lett. **120**, 243901 (2018).
32. Z. Chai, X. Hu, Y. Zhao, Y. Wu, S. Wang, H. Yang, and Q. Gong, AIP Adv. **8**, 65324 (2018).
33. G. Song, C. Zhang, Q. Cheng, Y. Jing, C.-W. Qiu, and T. J. Cui, Opt. Express **26**, 22916 (2018).
34. H. Li, C. Zhou, S. Wang, Y. Lu, and X. Xiang, Opt. Express **26**, 12742 (2018).
35. J. Xu, M. Cua, E. H. Zhou, Y. Horie, A. Faraon, and C. Yang, Opt. Lett. **43**, 5255 (2018).
36. G. Zheng, W. Wu, Z. Li, S. Zhang, M. Q. Mehmood, P. He, and S. Li, Opt. Lett. **42**, 1261 (2016).
37. X. Chen, L. Huang, M. Holger, G. Li, B. Bai, Q. Tan, G. Jin, C.-W. Qiu, S. Zhang, and Z. Thomas, Nat. Commun. **3**, 1198 (2012).
38. S. Bernet, W. Harm, and M. Ritschmarte, Opt. Express **21**, 6955 (2013).
39. S. Bernet and M. Ritschmarte, Opt. Express **25**, 2469 (2017).
40. L. Verslegers, P. B. Catrysse, Z. Yu, J. S. White, E. S. Barnard, M. L. Brongersma, and S. Fan, Nano Lett. **9**, 235 (2009).
41. X. Yin, H. Zhu, H. Guo, M. Deng, T. Xu, Z. Gong, X. Li, and Z. Hang, Laser Photonics Rev. **13**, 1800081 (2018).